DOI: 10.1002/((please add manuscript number))
Article type: Communication

Outstanding Indoor Performance of Perovskite Photovoltaic Cells – Effect of Device Architectures and Interlayers

*Harrison Ka Hin Lee† Jérémy Barbé,† Simone M. P. Meroni, Tian Du, Chieh-Ting Lin, Adam Pockett, Joel Troughton, Sagar M. Jain, Francesca De Rossi, Jennifer Baker, Matthew J. Carnie, Martyn A. McLachlan, Trystan M. Watson, James R. Durrant, and Wing C. Tsoi**

† These authors contributed equally in this work.

Dr. H. K. H. Lee, Dr. J. Barbé, S. M. P. Meroni, Dr. A. Pockett, Dr. J. Troughton, Dr. S. M. Jain, Dr. F. De Rossi, Dr. J. Baker, Dr. M. J. Carnie, Prof. T. M. Watson, Prof. J. R. Durrant, Dr. W. C. Tsoi
SPECIFIC, College of Engineering, Fabian Way, Bay Campus, Swansea University, Swansea SA1 8EN, UK
E-mail: w.c.tsoi@swansea.ac.uk
T. Du, C.-T. Lin, Dr. M. A. McLachlan, Prof. James R. Durrant
Department of Materials and Centre for Plastic Electronics, Imperial College London, South Kensington, London SW7 2AZ, UK
Prof. James R. Durrant
Department of Chemistry and Centre for Plastic Electronics, Imperial College London, South Kensington, London SW7 2AZ, UK

Keywords: Indoor photovoltaic, Internet of Things, perovskite photovoltaic, leakage current

Abstract

Indoor photovoltaics is one of the best sustainable and reliable energy source for low power consumption electronics such as the rapidly growing Internet of Things. Perovskite photovoltaic (PPV) cells with three benchmark device architectures – mesoporous PPV (mPPV) and inverted PPV (iPPV) with alternative hole transporting layers (HTLs), and carbon-based PPV (cPPV) are studied under simulated indoor environment. The mPPV cell using typical Spiro-OMeTAD as HTL shows the highest maximum power density (P_{max}) of 19.9 μW/cm^2 under 200 lux and 115.6 μW/cm^2 under 1000 lux (without masking), which is among the best of the indoor PV. Interestingly, when PTAA is used as HTL in mPPV cell, the P_{max} drops to almost zero under indoor light environment while its performance under one sun remains similar. On the other hand, when PEDOT:PSS is replaced by Poly-TPD as HTL in

iPPV cell, the P_{max} under indoor light improves significantly and is comparable to that of the best mPPV cell. This significant difference in indoor performance correlates well with their leakage current. The HTL-free cPPV cell, prepared by fully up-scalable techniques, shows promising P_{max} of 16.3 μW/cm^2 and 89.4 μW/cm^2 under 200 and 1000 lux, respectively. A practical scale 5cm × 5cm cPPV module is fabricated as a demonstration for real applications.

Indoor photovoltaics (PV) has drawn much attention in recent years due to the prospect of powering low power consumption electronics such as the Internet of Things which has been growing rapidly worldwide, and industry has forecasted to reach 30 billion devices in 2020 and 75 billion devices in 2025.[1] Sensors, wireless nodes, small displays, etc. are all low power consumption especially in sleep mode operation, from nanowatts to milliwatts, which could be supplied locally by PV devices via harvesting light from indoor environments.[2–6] These small electronics play an essential role for constructing future environments such as smart building as well as next generation factory and retail market.[7] For instance, electronic price tags with indoor PV devices embedded as a power source are wirelessly connected to a central computing system where individual prices can be controlled and updated via the wireless network. Similar concepts could be applied in most buildings and manufacturing lines where lots of sensors are required for monitoring and interacting purposes.

Despite the remarkable success of silicon-based PV for the outdoor use, this technology is not ideal for indoor light harvesting because of its poor performance under low light intensity.[6,8,9] III-V semiconductor PV is perhaps a better option for this application.[6,8,10] Mathews et al. showed that GaInP PV cells generate a P_{max} of 15.6 μW/cm^2 under 200 lux and 92.6 μW/cm^2 under 1000 lux of fluorescent lamps while amorphous silicon PV cells only generate roughly half of the P_{max} under the same testing conditions.[8] We note that researchers in the indoor PV community usually report and compare maximum power

density (P_{max}) instead of power conversion efficiency (PCE) because the intensity measurement for such a low light level could be error-prone. However, for indoor applications, III-V semiconductor PV is still much less popular than silicon-based PV because of its much higher production costs. Recently, indoor performance of several emerging PV technologies such as dye-sensitized and organic PV, have been explored and shown promising indoor performance.[11–17] They not only have promising potential to be much lower cost than the silicon PV cells, but also have significantly better indoor performance. Indeed, for dye-sensitized PV cells and organic PV cells, P_{max} up to 17.5 μW/cm^2 and 14.6 μW/cm^2 under 200 lux, and 101 μW/cm^2 and 78 μW/cm^2 under 1000 lux have been shown, respectively.[12,15]

In recent years, perovskite PV (PPV) cell, which is solution-processable with low material cost, have exhibited impressive improvement in PCE and reached over 20 % under standard one sun testing condition.[18,19] Both conventional mesoporous TiO_2 type PPV (mPPV) cells and the inverted type PPV (iPPV) cells had achieved high PCE under one sun illumination. Later, a hole transport layer (HTL) free mesoporous carbon stack device architecture was developed for PPV with slightly lower performance.[20] It consists of 3 consecutive stacks of mesoporous layers of TiO_2, ZrO_2 and carbon with perovskite infiltrated. This carbon electrode based PPV (cPPV) device architecture is highly compatible with up-scalable techniques. Furthermore, it is endowed with remarkable device stability and low cost in both materials and manufacturing.[21] However, cPPV devices usually possess higher series resistance (R_S) due to the lower conductivity of the carbon electrode, and therefore inferior one sun performance as compared to other device architectures. Both conventional and inverted PPV devices have been studied under indoor conditions, with remarkable P_{max} under indoor conditions.[22–24] However, their indoor performance could be poor if there is no further optimization of the electron transporting layer (ETL). Giacomo et al. showed that P_{max} of mPPV cells at 200 lux can be boosted from 0.3 to 15.4 μW/cm^2 after using atomic layer

deposition for the compact TiO_2 layer.[22] Chen et al. showed that the P_{max} of iPPV cells at 1000 lux can reach ~87 $\mu W/cm^2$ by additional spin-coating of the ETL.[23] To date, the highest P_{max} reported is 20.2 $\mu W/cm^2$ under 200 lux which employs conventional planar device structure with SnO_2 and MgO as dual ETL.[25]

The indoor performance of cPPV devices, and the effect of device architecture and HTL have not been explored in detail. To gain insight into the effect of the device architecture and the choice of HTL, here we study the indoor performance of methylammonium lead iodide (MAPI) based PPV cells by employing 3 common types of device architecture: (1) mPPV type, (2) iPPV type and (3) cPPV type, as illustrated in **Figure 1a**. 2,2',7,7'-Tetrakis[N,N-di(4-methoxyphenyl)amino]-9,9'-spirobifluorene (Spiro-OMeTAD) or poly[bis(4-phenyl)(2,4,6-trimethylphenyl)amine (PTAA) is used as HTL in mPPV devices while poly(3,4-ethylenedioxythiophene) polystyrene sulfonate (PEDOT:PSS) or poly(N,N'-bis-4-butylphenyl-N,N'-bisphenyl)benzidine (Poly-TPD) is used as HTL in the iPPV devices. PTAA and Poly-TPD were used because of higher one sun PCE demonstrated.[18,26]

Results and Discussion

PPV cells with different device architectures and the HTLs were studied under AM1.5G (one sun) condition as a reference. Figure 1b shows the best J-V characteristics of the device architectures and interlayers used for the PPV cells under one sun (all the device parameters are shown in **Table 1** and the external quantum efficiency spectra are available in Figure S1). The iPPV cell with PEDOT:PSS shows PCE of 12.2 %. By replacing the PEDOT:PSS with Poly-TPD, the PCE was improved significantly to 17.0 % due to enhanced short-circuit current density (J_{sc}) and open-circuit voltage (V_{oc}). The mPPV cells, with either Spiro-OMeTAD or PTAA, show PCE of over 14 %, while the cPPV cell shows PCE up to 11.2 %. The lower PCE of the cPPV cell is partly due to the higher series resistance (R_s) and

thus poorer fill factor (FF) originated from less conductive nature of the mesoporous carbon electrode when compared to the metal electrode used in the other device architectures.

The cells were then studied under fluorescent lamps (from 200 lux to 1000 lux) which mimics typical indoor environments. No masking was applied to the mPPV and iPPV devices during the J-V characterization as the mask will block some of the incoming light which is uncollimated in the indoor PV characterisation box. (Illustration is available in **Schematic diagram S1**) This indoor lighting has a narrow band emission mainly in the visible region (see Figure S2 for the spectrum and the image of the indoor light source) and its light intensity is about 3 orders of magnitude lower then the standard one sun spectrum. In contrast to their one sun performance, they show more diverse behaviour at low light level as shown in Figure 1c and 1d for measurement done under 1000 lux and 200 lux, respectively. The corresponding device parameters are listed in Table 1 (Data at 600 lux are also available in Figure S3 and Table S1). Both the mPPV cells using Spiro-OMeTAD and the iPPV cells using Poly-TPD show P_{max} of over 110 $\mu W/cm^2$ under 1000 lux and over 19 $\mu W/cm^2$ under 200 lux. Remarkably, both the mPPV-Spiro-OMeTAD and iPPV-Poly-TPD devices show one of the best P_{max} even without any modification to the ETL, suggesting that additional ETL or treatment may not be neccessary. The cPPV cells and the iPPV cells using PEDOT:PSS show moderate P_{max} of 16.3 $\mu W/cm^2$ and 9.0 $\mu W/cm^2$ under 200 lux, and 89.4 $\mu W/cm^2$ and 77.5 $\mu W/cm^2$ under 1000 lux, respectively. The mPPV cells using PTAA have much lower P_{max} of 1.2 $\mu W/cm^2$ under 200 lux and 16.1 $\mu W/cm^2$ under 1000 lux. It is important to note that both the mPPV cells, using Spiro-OMeTAD and PTAA as HTL, show similar performance under one sun but perform opposingly under low light levels.

To have better undertanding of the variation in the performance under the low light conditions, the dark current of different device architectures with the HTLs were studied which is closely related to the leakage current in the device.[27] As shown in **Figure 2a**, the

magnitude of the leakage current (current taken at -0.2 V) has the order: mPPV-PTAA > iPPV-PEDOT:PSS > mPPV-Spiro-OMeTAD and cPPV > iPPV-Poly-TPD. For devices having high leakage current like the mPPV-PTAA cells and the iPPV-PEDOT:PSS cells, the leakage current could dominate the photocurrent when the incident light intensity is low, resulting in poor device performance.[22,28] In other words, if the leakage current is higher than or has the same order of magnitude as the photocurrent, ie. 0.02-0.04 mA/cm^2 under 200 lux or 0.1-0.2 mA/cm^2 under 1000 lux, the overall current are dominated or disturbed by the leakage current resulting in much lower FF and V_{OC}. For cells with low leakage current, like the mPPV cells using Spiro-OMeTAD, iPPV cells using Poly-TPD and cPPV cells, their PV characteristic are retained under low light condition. In brief, a leakage current below 10^{-3} mA/cm^2 is recommended for devices operating under typical indoor condition.

Apart from the leakage current, the shunt resistance (R_{Sh}) is perhaps another indicative parameter to look at for low light applications. Using either organic solar cells or PPV cells, a few works suggested that a high shunt resistance is required for devices to perform well under low light intensity.[22,24,29,30] However, Lechêne et al. showed that the shunt resistance itself may not be enough to determine how a PV device performs under low light level.[28] Similar to their finding, the R_{Sh} values (available in Table S2) of the devices studied herein do not show a clear trend with the performance, suggesting that probing the dark current of the devices should give better indications for the low light behaviour.

The V_{OC} is a key parameter to look at especially for indoor PV.[31] Diode ideality factor (n) can reveal how the V_{OC} drop with decreasing light intensity. The diode ideality factors of the various device architectures and HTLs are calculated from the plot of V_{OC} as a function of light intensity under solar spectrum, which is shown in Figure 2b. In most cases, the data follow the equation below derived from the Shockley diode equation:

$$V_{OC} \sim \frac{nkT}{e} \ln\left(\frac{I_{ph}}{I_0}\right) \quad (1)$$

where k is the Boltzmann constant, T is the absolute temperature, e is the elementary charge, I_{ph} is the photocurrent and I_0 is the saturation current of the diode. By fitting the V_{oc} data to the equation, we can obtain the slope and thus extract the values of n which has the order: mPPV-PTAA cell (n = 2.60) > iPPV-Poly-TPD cell (n = 1.52) and the cPPV cell (n = 1.62) > mPPV-Spiro-OMeTAD (n = 1.36) cell and iPPV-PEDOT:PSS cell (n = 1.37). The high diode ideality factor extracted for the mPPV-PTAA cell could be affected by the low shunt resistance which makes it no longer linear at lower light intensity.[28] To achieve higher V_{OC} at low light intensity, the V_{OC} at one sun could play a more significant role than the diode ideality factor provided that devices possess reasonable value of n lying between 1 and 2. For PPV cells, interfacial engineering is particularly useful for boosting the V_{OC}. As shown here, by replacing the PEDOT:PSS layer with Poly-TPD in the iPPV devices, the V_{OC} was enhanced by 0.150 V at 1 sun, 0.063 V at 1000 lux and 0.453 V at 200 lux.

Here, we introduce a ratio of the P_{max} at 1000 lux to the P_{max} at one sun ($P_{max,1000lux}/P_{max,1sun}$) to compare the change in performance from one sun to 1000 lux condition for all these PPV cells as shown in Figure 2c. This parameter can reveal the change in the overall performance from one sun to fluorescent lamps of 1000 lux. The ratios for all the devices are calculated and results in the following order: cPPV (7.9×10^{-3}) > mPPV-Spiro-OMeTAD (7.7×10^{-3}) > iPPV-Poly-TPD (6.6×10^{-3}) > iPPV-PEDOT:PSS (5.6×10^{-3}) > mPPV-PTAA (1.1×10^{-3}). Unexpectedly, the cPPV cells show the highest ratio among all the PPV cells, provided that the performance of cPPV cell is not particularly outstanding under the indoor condition. We attempted to find a corelation between the device parameters and the ratios and found that the values of $P_{max,1000lux}/P_{max,1sun}$ corelate well to the series resistance (R_S) of the devices as plotted in the same figure (R_S values are available in Table S2). A higher ratio corresponds to a higher R_S. This correlation can be explained by the fact that a high R_S has a bigger impact on the device performance under one sun (reduction in the FF) than under low light level.[29] In other words, there is much higher tolerance to the R_S

when the operating current is much lower such as the one under indoor lighting.[29] As demonstrated here, the cPPV cell has a high R_S value leading to a significantly lower FF under one sun (58 %), However, this high R_S does not hinder the FF under low light (71.9 % for 1000 lux and 70.4 % for 200 lux). It suggests that devices having higher R_S can perform relatively better at low light level, like the cPPV cells in this study.

The cPPV cells are distinct from the mPPV and iPPV cells. The triple mesoporous stack of TiO_2, ZrO_2 and carbon are all prepared by screen printing which allows sheet-to-sheet manufacturing. It has been demonstrated that cPPV cell is low cost and has excellent stability with no loss in PCE under controlled one sun condition for over 10000 hours.[21] We anticipated that the stability under indoor light operation is likely to be significantly longer as the stress conditions are much milder: UV and infrared free, much lower light intensity, operation at room temperature and in indoor environment. Besides, the indoor performance is remarkable as shown earlier. With this exciting prospect, we have fabricated a 5 cm × 5 cm cPPV module with active area of 9.75 cm^2 as a demonstration, using the same scalable methods as the small cPPV cells (1 cm^2). As shown in Figure 2d, it has a maximum power of 683 µW under 1000 lux, which corresponds to P_{max} of 70.1 µW/cm^2, significantly better than silicon PV module reported elsewhere (P_{max} of ~15 – 46 µW/cm^2 under 1000 lux).[6,8,32] The FF of the module is over 70 % at 1000 lux, suggesting that the high R_S, even in a practical size module, is still within the tolerance (one sun data of the module is available in Figure S4). Such a high tolerance in R_S implies higher flexibility on the design of the inter-connection between subcells in a module to be operated under low light environment.

The comparison of the different device architectures together with different HTLs give deeper insight on designing PPV for indoor applications. For example, by changing only the HTL of the mPPV cells from Spiro-OMeTAD to PTAA, even if the PCE under one sun remain similar, the leakage current can be increased by 3 orders of magnitude, leading to dramatic difference in the performance under low light. For iPPV cells, in addition to the

suppressed leakage current when Poly-TPD is used as the HTL instead of PEDOT:PSS, there is a considerable enhancement in the V_{OC} under both high and low light conditions which is important for low light performance especially when devices have low diode ideality factor. Note that the PCE under one sun of the mPPV and iPPV reported here is not the highest among the reported values, and therefore, with state-of-the-art PPV devices under one sun, the P_{max} under low light could be even higher.

Statistical study of the device performance and the stabilized P_{max} study were performed for the best devices in each category under 1000 lux (See Table S3 and Figure S5). In general, the mPPV and cPPV devices show more cell-to-cell variation than the iPPV device which could be due to the less controlled preparation methods – the spray-coated compact TiO_2 layer in the mPPV cells and the screen printed layers in the cPPV cells. The iPPV cells are not only statically better than the mPPV and cPPV cells but also better in the stabilized P_{max} measurement. The iPPV-Poly-TPD cell reaches its stabilized P_{max} of 109 $\mu W/cm^2$ almost instantaneously with the performance similar to the extracted value from the J-V scans while the mPPV-Spiro-OMeTAD and cPPV cells take about 60 and 180 s to stabilize, with slightly lower P_{max} of 101 and 75 $\mu W/cm^2$, respectively. This difference in stabilization time correlates well with their hysteresis under low light conditions, in which iPPV-Poly TPD devices show almost no hysteresis under low light while mPPV-Spiro-OMeTAD and cPPV devices have certain hysteresis (see Figure 1c and 1d). The elimination of the hysteresis for the iPPV-Poly TPV device can be ascribed to the passivation effect of Poly-TPD at the interface, similar to the passivation effect of PCBM at the other interface of the perovskite film.[33,34] It is also worth noting that the hysteresis seems to increase with decreasing light intensity (comparing Figure 1b, 1c and 1d), which could be explained by relatively larger contribution from the movement of mobile ions when the photogenerated current is lower under low light level.

Conclusions

In summary, PPV cells using 3 types of device architectures were studied under indoor lighting conditions and showed substantial difference in their performance depending on the choice of interlayer. The mPPV-Spiro-OMeTAD and iPPV-Poly-TPD cells show maximum power density of over 111 μW/cm^2 under 1000 lux and over 19 μW/cm^2 under 200 lux, which are one of the highest among all kind of reported PV devices. The performance under low light intensity correlates well with the leakage current, and a maximum leakage current of 10^{-3} mA/cm^2 is suggested to avoid influencing the performance at low light intensity. Considering the reasonable indoor performance of the cPPV cell and module (5 cm × 5 cm module with P_{max} = 70.0 μW/cm^2 under 1000 lux), which are fully up-scalable as demonstrated here, together with its low cost and promising stability, we believe that cPPV is the readiest device architecture to be commercialized for low light applications. We envision that PPV cells should have enormous potential and impact to the indoor PV market.

Experimental Section

Fabrication of mPPV cells:

Titanium diisopropoxide bis(acetylacetonate) solution (Aldrich) was spin-coated on fluorine doped tin oxide (FTO) coated glass substrates and annealed at 400 °C for 30 minutes to form compact TiO_2 layers. Diluted mesoporous TiO_2 paste (Dyesol) was spin-coated onto the substrates and annealed at 450 °C for 30 minutes. Then, 0.1 M bis(trifluoromethane) sulfonimide lithium salt (Li-TFSI) in acetonitrile were loaded (10 seconds) and spin-coated onto the substrates to passivate the mesoporous-TiO_2 surface, and then annealed at 450 °C for 30 minutes. Then, 1.5M $CH_3NH_3PbI_3$ precursor solution in DMF and DMSO (9:1 in volume) was spin-coated onto the samples and then annealed at 100 °C for 10 minutes. Spiro-OMeTAD (Borun New Material Technology) or PTAA (Ossila) were dissolved in chlorobenzene and doped with Li-TFSI and 4-tert-butylpyridine and spin-coated onto the

perovskite layer. Finally, the mPPV cells were finished by thermally evaporating 100 nm of Au onto the samples, forming an active area of 0.08-0.10 cm^2 for each cell.

Fabrication of iPPV cells:

PEDOT:PSS or Poly-TPD (0.25 wt% in chlorobenzene) were spin-coated onto indium-doped tin oxide (ITO) substrates. PEDOT:PSS films are dried at 150 °C for 15 minutes. For Poly-TPD films, they are dried for 1 minute before spin-coating an ultrathin poly[(9,9-bis(3'-(N,N-dimethylamino)propyl)-2,7-fluorene)-alt-2,7-(9,9-dioctylfluorene)] (PFN) layer (0.05 wt% in methanol) onto the Poly-TPD layer for better wettability.[26] 1.5 M $CH_3NH_3PbI_3$ precursor solution in DMF and DMSO (9:1 in volume) was spin-coated onto the samples and, during the spin-coating, diethy ether was dripped onto the substrates. The substrates were then annealed on a 100 °C hot plate for 15 minutes. After cooling down, PCBM solution was spin-coated on the MAPI films. Finally, the devices were completed by thermally evaporating 0.7 nm of LiF and 100 nm of Ag PCBM layer, forming an active area of 0.045 cm^2 for each cell.

Fabrication of cPPV cells:

A compact TiO_2 layer was deposited by spray pyrolysis (25 sprays every 10 s at 300 °C) with a 10 % solution of TAA (diluted in 2-propanol). Mesoporous layers of titania (TiO_2), zirconia (ZrO_2) and carbon were screen printed and annealed one by one at 550 °C for TiO_2 and 400 °C for ZrO_2 and carbon. The TiO_2 paste was diluted in terpineol in a 1:1 ratio by weight, whereas the other pastes were used as bought. The AVA-MAPI precursors solution was prepared with 439.0 mg, 151.4 mg and 6.7 mg of respectively PbI_2, MAI, and 5-AVAI in 1 mL of γ-Butyrolactone. The solution was then deposited with the so-called Robotic Mesh method.[35] In this Robotic Mesh method, a robotic dispenser moves a syringe to continuously deliver the precursor solution at 12 m/s to a mesh which is on the top of the device to

homogeneously spread the liquid on the surface. The wet devices were kept in a petri dish for 10 minutes at room temperature and then heated at 50 °C in oven. After 60 minutes, the petri dish was opened and the devices were left in the oven for another hour for a complete drying step. The devices were then placed in humidity oven at relative humidity of 70 % and 25 °C similarly as reported elsewhere.[36] The scribes were performed mechanically with a steal blade for the contact aperture and the cell disconnection according to the scribing method.[37] The resulting area of the cPPV cell and module are 1 cm^2 and 9.75 cm^2, respectively. A mask with an openning of 0.49 cm^2 was applied for the cPPV cells during the measurement.

J-V characterization:

J-V characterizations were performed by a Keithley 2400 sourcemeter under a solar simulator and a series of fluorescent lamps (Osram L18W/827) with reflectors. Different illuminance are obtained by adjusting the power supplied to the fluorescent lamps. The distance between the light source and the devices were kept constant. The indoor light source was calibrated by a luxmeter, LX-1330B and a power and energy meter (Thorlabs PM100D) equipped with a high-sensitivity thermal sensor (Thorlabs S401C). V_{OC} at different light intensity were obtained by measuring the J-V characteristics under the solar simulator using a set of optical density filters. No mask was applied to the mPPV and iPPV cells for all the J-V characterization.

Supporting Information
Supporting Information is available from the Wiley Online Library or from the author.

Acknowledgements
The authors would like to acknowledge the funding support from the Welsh Assembly Government funded Sêr Cymru Solar Project, EPSRC (grant no. EP/M025020/1), the European Union's Horizon 2020 research and innovation programme under the Marie Skłodowska-Curie grant (agreement no. 663830), the Self-assembling Perovskite Absorbers –

Cells Engineered into Modules project through EPSRC (grant no. EP/M015254/2) and the SPECIFIC Innovation and Knowledge Centre (EP/N020863/1).
H. K. H. Lee and J. Barbé contributed equally to this work.

Received: ((will be filled in by the editorial staff))
Revised: ((will be filled in by the editorial staff))
Published online: ((will be filled in by the editorial staff))

Author contributions

Device fabrication was carried out by J. B., S. M. P. M., T. D. C-T. L., A.P., J.T., S. M. J., F. D. R. and J. B. Device characterization were carried out by H. K. H. L., J.B., and S. M. P. M. H. K. H. L., J.B., M. J. C., M. A. M., T. M. W., J. R. D. and W. C. T. contributed to project planning and discussions. W. C. T. H. K. H. L. and J. B. had the idea, led the project, and prepared the manuscript. All authors contributed to the manuscript preparation.

References

[1] "Internet of Things (IoT) connected devices installed base worldwide from 2015 to 2025 (in billions)," **n.d.**
[2] H. Jayakumar, K. Lee, W. S. Lee, A. Raha, Y. Kim, V. Raghunathan, in *Proc. 2014 Int. Symp. Low Power Electron. Des.*, **2014**, pp. 375–380.
[3] A. Nasiri, S. A. Zabalawi, G. Mandic, *IEEE Trans. Ind. Electron.* **2009**, *56*, 4502.
[4] M. Gorlatova, P. Kinget, I. Kymissis, D. Rubenstein, X. Wang, G. Zussman, *IEEE Wirel. Commun.* **2010**, *17*, 18.
[5] K. Niotaki, A. Collado, A. Georgiadis, S. Kim, M. M. Tentzeris, *Proc. IEEE* **2014**, *102*, 1712.
[6] A. S. Teran, S. Member, J. Wong, S. Member, W. Lim, S. Member, G. Kim, Y. Lee, D. Blaauw, J. D. Phillips, S. Member, *IEEE Trans. Electron Devices* **2015**, *62*, 2170.
[7] J. W. Matiko, N. J. Grabham, S. P. Beeby, M. J. Tudor, *Meas. Sci. Technol.* **2014**, *25*, 012002.
[8] I. Mathews, P. J. King, F. Stafford, R. Frizzell, *IEEE J. Photovoltaics* **2016**, *6*, 230.
[9] N. H. Reich, W. G. J. H. M. van Sark, W. C. Turkenburg, *Renew. Energy* **2011**, *36*, 642.
[10] I. Mathews, G. Kelly, P. J. King, R. Frizzell, in *2014 IEEE 40th Photovolt. Spec. Conf.*, **2014**, pp. 0510–0513.
[11] M. Freitag, J. Teuscher, Y. Saygili, X. Zhang, F. Giordano, P. Liska, J. Hua, S. M. Zakeeruddin, J.-E. Moser, M. Grätzel, A. Hagfeldt, *Nat Phot.* **2017**, *11*, 372.
[12] Y. Cao, Y. Liu, S. M. Zakeeruddin, A. Hagfeldt, M. Grätzel, *Joule* **2018**, *2*, 1108.
[13] H. K. H. Lee, Z. Li, J. R. Durrant, W. C. Tsoi, *Appl. Phys. Lett.* **2016**, *108*, 253301.
[14] S. Yang, Z. Hsieh, M. L. Keshtov, G. D. Sharma, F. Chen, *Sol. RRL* **2017**, *1*, 1700174.
[15] H. K. H. Lee, J. Wu, J. Barbé, S. M. Jain, S. Wood, E. M. Speller, Z. Li, F. A. Castro, J. R. Durrant, W. C. Tsoi, *J. Mater. Chem. A* **2018**, *6*, 5618.
[16] H. Yin, J. K. W. Ho, S. H. Cheung, J. R. Yan, K. L. Chiu, X. Hao, S.-K. So, *J. Mater. Chem. A* **2018**, *6*, 8579.
[17] N. Teng, S. Yang, F. Chen, *IEEE J. Photovoltaics* **2018**, *8*, 752.
[18] W. S. Yang, B.-W. Park, E. H. Jung, N. J. Jeon, *Science* **2017**, *356*, 1376.
[19] X. Zheng, B. Chen, J. Dai, Y. Fang, Y. Bai, Y. Lin, H. Wei, X. C. Zeng, J. Huang, *Nat. Energy* **2017**, *2*, 17102.
[20] A. Mei, X. Li, L. Liu, Z. Ku, T. Liu, Y. Rong, M. Xu, M. Hu, J. Chen, Y. Yang, M. Grätzel, H. Han, *Science* **2014**, *345*, 295.

[21] G. Grancini, C. Roldán-Carmona, I. Zimmermann, E. Mosconi, X. Lee, D. Martineau, S. Narbey, F. Oswald, F. De Angelis, M. Graetzel, M. K. Nazeeruddin, *Nat. Commun.* **2017**, *8*, 15684.
[22] F. Di Giacomo, V. Zardetto, G. Lucarelli, L. Cinà, A. Di Carlo, M. Creatore, T. M. Brown, *Nano Energy* **2016**, *30*, 460.
[23] C. Y. Chen, J. H. Chang, K. M. Chiang, H. L. Lin, S. Y. Hsiao, H. W. Lin, *Adv. Funct. Mater.* **2015**, *25*, 7064.
[24] J. Dagar, S. Castro-Hermosa, M. Gasbarri, A. L. Palma, L. Cina, F. Matteocci, E. Calabrò, A. Di Carlo, T. M. Brown, *Nano Res.* **2018**, *11*, 2669.
[25] J. Dagar, S. Castro-Hermosa, G. Lucarelli, F. Cacialli, T. M. Brown, *Nano Energy* **2018**, *49*, 290.
[26] J. Lee, H. Kang, G. Kim, H. Back, J. Kim, S. Hong, B. Park, E. Lee, K. Lee, *Adv. Mater.* **2017**, *29*, 1606363.
[27] C. M. Proctor, T. Q. Nguyen, *Appl. Phys. Lett.* **2015**, *106*, 083301.
[28] B. P. Lechêne, M. Cowell, A. Pierre, J. W. Evans, P. K. Wright, A. C. Arias, *Nano Energy* **2016**, *26*, 631.
[29] R. Steim, T. Ameri, P. Schilinsky, C. Waldauf, G. Dennler, M. Scharber, C. J. Brabec, *Sol. Energy Mater. Sol. Cells* **2011**, *95*, 3256.
[30] Y. Zhou, T. M. Khan, J. W. Shim, A. Dindar, C. Fuentes-Hernandez, B. Kippelen, *J. Mater. Chem. A* **2014**, *2*, 3492.
[31] H. K. H. Lee, Z. Li, J. R. Durrant, W. C. Tsoi, *Appl. Phys. Lett.* **2016**, *108*, 253301.
[32] Y. Li, N. J. Grabham, S. P. Beeby, M. J. Tudor, *Sol. Energy* **2015**, *111*, 21.
[33] Y. Shao, Z. Xiao, C. Bi, Y. Yuan, J. Huang, *Nat. Commun.* **2014**, *5*, 1.
[34] K. Tvingstedt, L. Gil-Escrig, C. Momblona, P. Rieder, D. Kiermasch, M. Sessolo, A. Baumann, H. J. Bolink, V. Dyakonov, *ACS Energy Lett.* **2017**, *2*, 424.
[35] S. M. P. Meroni, Y. Mouhamad, F. De Rossi, A. Pockett, J. Baker, R. Escalante, J. Searle, M. J. Carnie, E. Jewell, G. Oskam, T. M. Watson, *Sci. Technol. Adv. Mater.* **2018**, *19*, 1.
[36] S. G. Hashmi, D. Martineau, M. I. Dar, T. T. T. Myllymäki, T. Sarikka, V. Ulla, S. M. Zakeeruddin, M. Grätzel, *J. Mater. Chem. A* **2017**, *5*, 12060.
[37] K. Kushiya, Y. Tanaka, H. Hakuma, Y. Goushi, S. Kijima, T. Aramoto, Y. Fujiwara, *Thin Solid Films* **2009**, *517*, 2108.

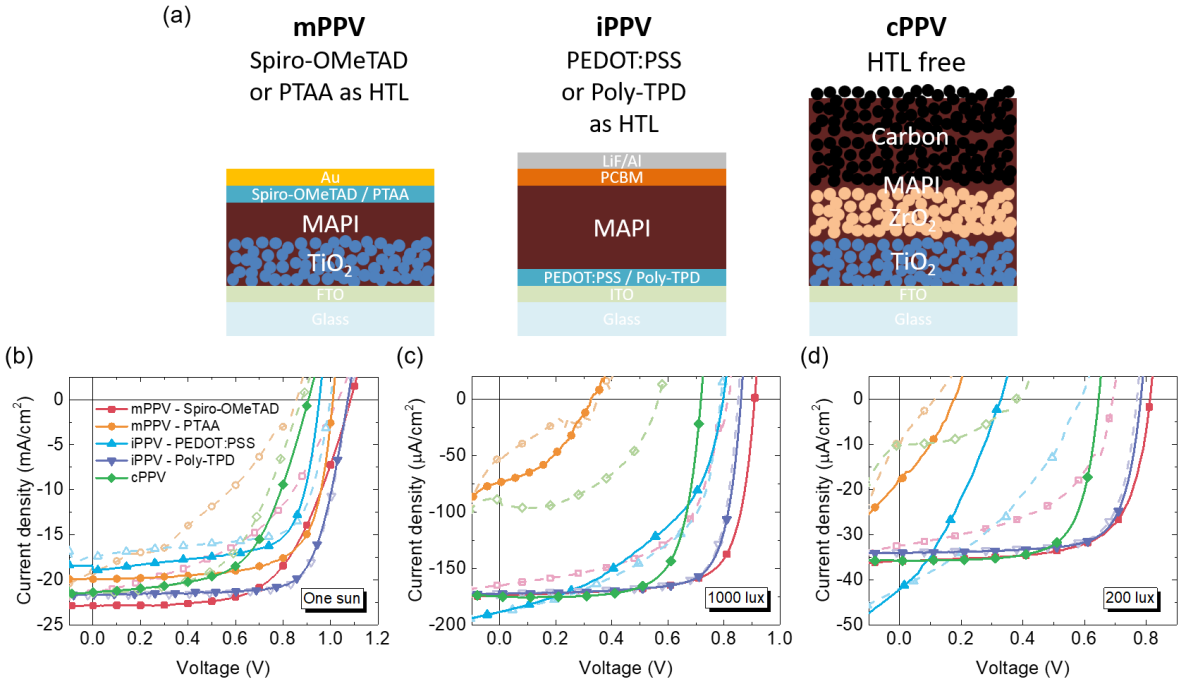

Figure 1 (a) Schematic diagram of 3 types of perovskite device architectures studied in this work. J-V characteristics under (b) one sun, (c) fluorescent lamps of 1000 lux and (d) fluorescent lamps of 200 lux. Solid lines and dash lines represent reverse and forward scan of the J-V measurements, respectively.

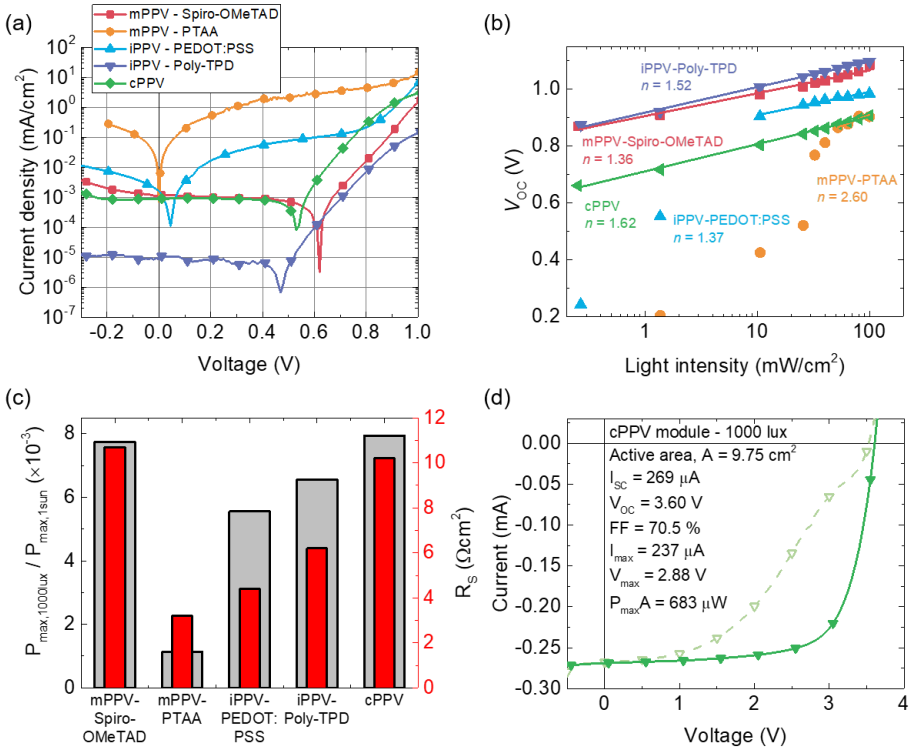

Figure 2 (a) Dark J-V characteristics, (b) V_{OC} measured at different light intensity under AM1.5G. (c) Ratios of $P_{max,1000lux}$ to $P_{max,1sun}$ and Rs of different PPV cells. (d) J-V characteristics (solid line for reverse scan and dash line for forward scan) of a 5 cm × 5 cm cPPV module with 5 subcells connected in series measured at 1000 lux.

Table 1 Device parameters of the best PPV cells measured under different lighting conditions.

	a)	One sun (P_{in} = 100 mW/cm^2)				1000 lux [200 lux]			
		J_{SC} (mA/cm^2)	V_{OC} (V)	FF (%)	PCE (%)	J_{SC} (μA/cm^2)	V_{OC} (V)	FF (%)	P_{max} (μW/cm^2)
mPPV-Spiro-OMeTAD	**R**	22.9	1.08	60.2	14.9	173.7 [35.8]	0.910 [0.812]	73.1 [68.4]	115.6 [19.9]
	F	21.4	1.03	1.03	10.0	165.2 [32.7]	0.814 [0.691]	56.3 [50.5]	75.7 [11.4]
mPPV-PTAA	**R**	19.9	1.01	70.4	14.2	85.6 [18.6]	0.472 [0.201]	36.0 [31.8]	16.1 [1.2]
	F	15.7	0.92	41.3	5.95	55.3 [10.3]	0.349 [0.114]	35.3 [21.5]	6.8 [0.3]
iPPV-PEDOT:PSS	**R**	18.9	0.95	67.9	12.2	188.7 [42.2]	0.797 [0.329]	45.2 [32.5]	68.0 [4.5]
	F	17.3	1.00	68.7	11.9	189.1 [42.0]	0.788 [0.589]	52.1 [36.4]	77.5 [9.0]
iPPV-Poly-TPD	**R**	21.6	1.07	73.6	17.0	172.5 [34.1]	0.860 [0.782]	75.4 [73.5]	111.9 [19.6]
	F	21.8	1.07	73.7	17.2	172.3 [33.9]	0.851 [0.770]	75.9 [73.7]	111.3 [19.2]
cPPV	**R**	21.4	0.91	58.0	11.2	174.9 [35.8]	0.718 [0.646]	71.9 [70.4]	89.4 [16.3]
	F	21.5	0.88	53.4	10.1	91.5 [10.6]	0.566 [0.380]	51.5 [42.7]	26.6 [1.7]

[a)] R stands for reverse scan and F stands for forward scan.

Table of contents

Perovskite photovoltaic (PPV) cells employing benchmark device architectures with alternative hole transporting layer (HTL) are studied under simulated indoor environment. With suitable combination of device architecture and HTL, maximum power density of over 19 μW/cm^2 and 110 μW/cm^2 under fluorescent lamps of 200 lux and 1000 lux are demonstrated, respectively. High potential of commercialization of a fully printable carbon-based PPV architecture is suggested via demonstration of practical size module.

Keyword

Indoor photovoltaic, Internet of Things, perovskite photovoltaic, leakage current

*Harrison Ka Hin Lee† Jérémy Barbé,† Simone M. P. Meroni, Tian Du, Chieh-Ting Lin, Adam Pockett, Joel Troughton, Sagar M. Jain, Francesca De Rossi, Jennifer Baker, Matthew J. Carnie, Martyn A. McLachlan, Trystan M. Watson, James R. Durrant, and Wing C. Tsoi**

Title

Outstanding Indoor Performance of Perovskite Photovoltaic Cells – Effect of Device Architectures and Interlayers

ToC figure

Supporting Information

Title
Outstanding Indoor Performance of Perovskite Photovoltaic Cells – Effect of Device Architectures and Interlayers

Harrison Ka Hin Lee,† Jérémy Barbé,† Simone M. P. Meroni, Tian Du, Chieh-Ting Lin, Adam Pockett, Joel Troughton, Sagar M. Jain, Francesca De Rossi, Jennifer Baker, Matthew J. Carnie, Martyn A. McLachlan, Trystan M. Watson, James R. Durrant, and Wing C. Tsoi*

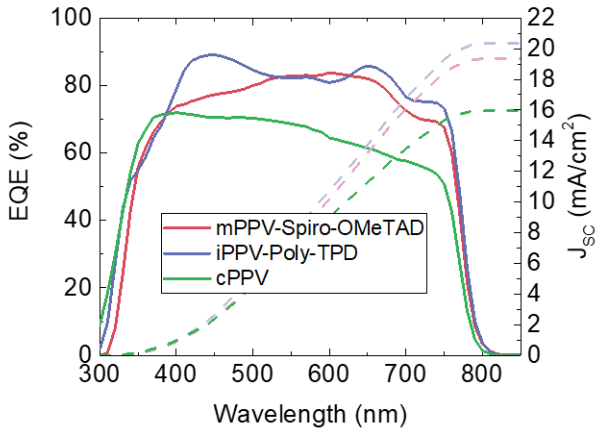

Figure S1 External quantrum efficiency with integrated J_{SC} values of the best PPV cell in each category.

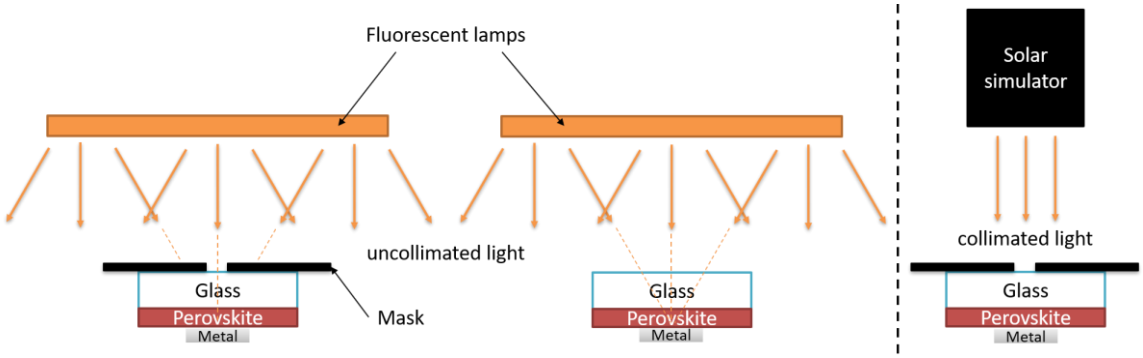

Schematic diagram S1 Illustration of how a mask blocks the uncollimated light from the fluorescent lamps during the indoor PV characterization. Since the thickness of the glass (1-2 mm in our devices) is comparable to the dimension of the device active area and the opening of the mask, part of the incoming light, which is not coming straightly above the active area from the fluorescent lamps, will be blocked by the mask and this results in underestimation of the photocurrent. However, it is not a problem in the situation of one sun characterization as the light from the solar simulator is usually collimated. To check the reliability of the device area used because of the absent of the mask, J_{SC} integrated from the EQE spectra were checked and they agreed with the J_{SC} obtained under one sun (see Figure S1).

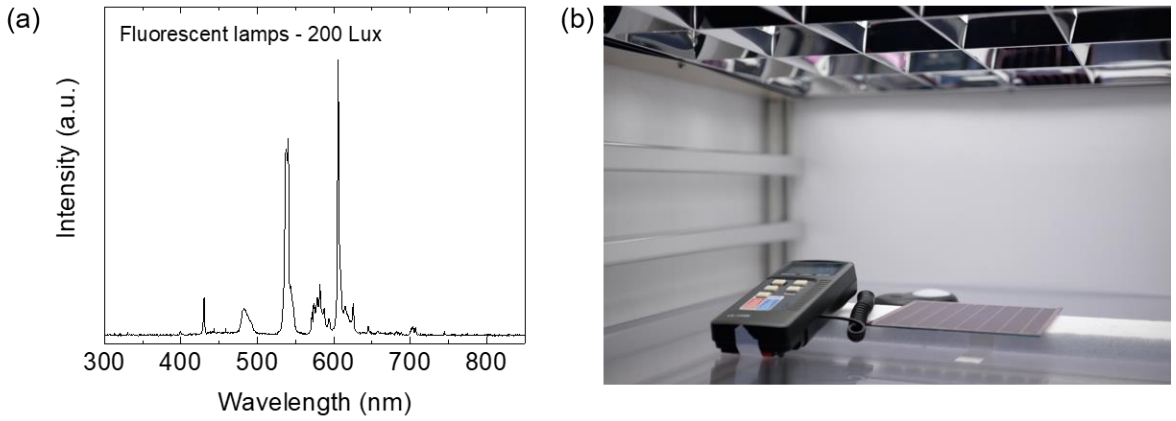

Figure S2 (a) Emission spectrum of the fluorescent lamps at 200 lux and (b) image of the indoor PV characterization box.

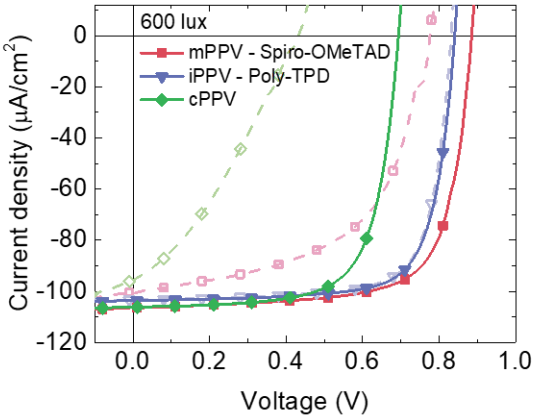

Figure S3 J-V characteristics of the best cell in each category under fluorescent lamps of 600 lux. Solid lines and dash lines represent reverse and forward scans of the J-V measurements, respectively.

Table S1 Device parameters of the best PPV cells in each category measured under fluorescent lamps of 600 lux.

	a)	J_{SC} (μA/cm²)	V_{OC} (V)	FF (%)	P_{max} (μW/cm²)
mPPV-Spiro-OMeTAD	R	106.6	0.885	72.3	68.2
	F	100.9	0.776	55.4	43.4
iPPV-Poly-TPD	R	103.6	0.841	74.6	65.0
	F	103.4	0.831	75.0	64.5
cPPV	R	106.2	0.694	70.2	51.7
	F	95.6	0.432	32.2	13.3

Table S2 Series resistance (R_S) and shunt resistance (R_{Sh}) of the PPV cells extracted from the reverse J-V scan under one sun.

	R_S (Ωcm²)	R_{Sh} (Ωcm²)
mPPV-Spiro-OMeTAD	10.7	1280
mPPV-PTAA	3.2	1201
iPPV-PEDOT:PSS	4.4	382
iPPV-Poly-TPD	6.2	2793
cPPV	10.2	646

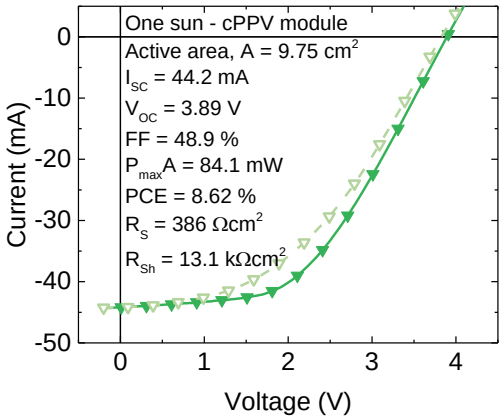

Figure S4 J-V characteristics of a 5 cm × 5 cm cPPV module measured under one sun. Solid lines and dash lines represent reverse and forward scan of the J-V measurements. Device parameters from the reverse scan are shown inside the figure.

Table S3 Average values of the device parameters obtained under 1000 lux for the best interlayer in each category. Their standard deviations are shown in the parentheses. The statistical data are obtained from 6-8 cells.

	a)	J_{SC} ($\mu A/cm^2$)	V_{OC} (V)	FF (%)	P_{max} ($\mu W/cm^2$)
mPPV-Spiro-OMeTAD	R	154.8 (13.8)	0.836 (0.049)	68.3 (3.4)	95.9 (1.6)
	F	129.6 (29.1)	0.735 (0.046)	40.5 (14.4)	45.9 (3.0)
iPPV-Poly-TPD	R	160.5 (11.6)	0.869 (0.008)	76.1 (1.8)	105.9 (4.6)
	F	160.1 (11.8)	0.864 (0.010)	76.3 (1.1)	105.3 (5.5)
cPPV	R	154.2 (15.7)	0.717 (0.019)	73.7 (5.2)	81.7 (11.7)
	F	96.6 (37.9)	0.559 (0.078)	40.9 (14.9)	23.1 (14.2)

a) R stands for reverse scan and F stands for forward scan.

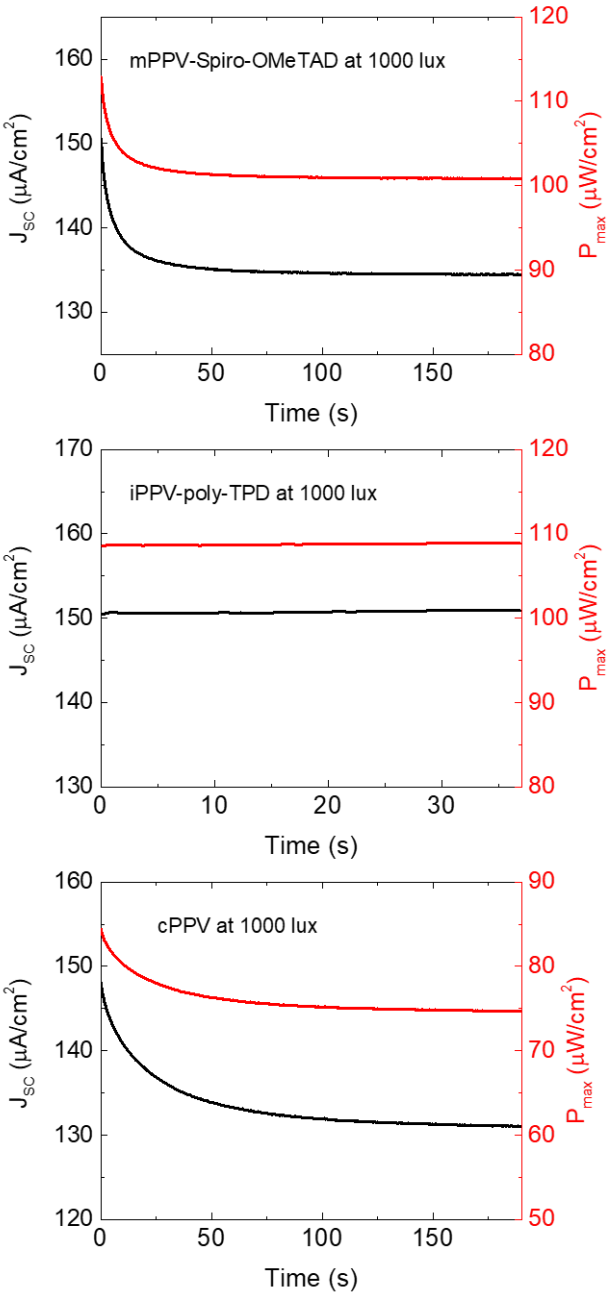

Figure S5 Stabilized measurements of the J_{SC} and the corresponding P_{max} at 1000 lux.